https://dx.doi.org/10.1016/j.ijheatmasstransfer.2021.121733

Enhancing the Cooling and Dehumidification Performance of Indirect Evaporative Cooler by Hydrophobic-coated Primary Air Channels

Yunran Min [a,*], Wenchao Shi [a], Boxu Shen [a], Yi Chen [b], Hongxing Yang [a,*]

a. Renewable Energy Research Group (RERG), Research Institute for Smart Energy (RISE), The Hong Kong Polytechnic University, Hong Kong

b. School of Mechanical and Energy Engineering, Jimei University, Fujian, China

Abstract

An indirect Evaporative Cooler (IEC) for air-conditioning (AC) energy recovery is a rapidly developing technology and has great potential applications in hot and humid regions. As the cooling potential of exhaust air is captured to evaporate the spraying water, the humid fresh air in adjacent channels can be cooled with moisture extracted. The condensation of fresh air can pose significant influences on the cooling and dehumidification performance of the cooler. However, the effect of surface modification on both sensible and latent heat transfer in dry channels of IEC was hardly discussed in the literature. In this paper, a novel IEC heat exchanger was proposed by depositing the hydrophobic nanoparticles on the surfaces of primary air channels. Visualized experiments were carried out to compare the condensation heat transfer mechanisms as well as the effects of influence factors on the performance of the hydrophobic-coated IEC and the traditional un-coated one. Results show that, larger irregular droplets drained off as water film was observed on the bare-aluminum plate, while the hydrophobic surface promoted dropwise condensation with a smaller droplet diameter. The minimized size of falling-off droplets and frequent droplet removal can enhance the convective heat transfer of the processed air flowing over the coated plate surface. The hydrophobic coating treatment on the primary air channel surfaces increased the energy-saving rate of IEC by 8.5-17.2%, which can potentially be utilized in AC applications under dehumidifying conditions.

Keywords: Indirect evaporative cooler; Condensation; Heat transfer; Hydrophobic surface

Nomenclature

A	surface area, m^2	γ	surface tension of liquid-vapor interface, N/m
c	specific heat, J/(kg·℃)	η	wet-bulb effectiveness
d_e	hydraulic diameter of channel, m	θ	equilibrium contact angle, °
g	gravity acceleration, m^2/s	λ	thermal conductivity, W/(m·℃)
h	heat transfer coefficient, W/(m^2·℃)	μ	dynamic viscosity, Pa·s
h_m	mass transfer coefficient, kg/(m^2·s)	σ_l	water surface tension, J/kg

* Corresponding author.

E-mail address: yunran.min@connect.polyu.hk (Y. Min) and hong-xing.yang@polyu.edu.hk (H. Yang)

i_{lv}	latent heat of water vapor, J/kg	ρ	liquid density, kg/m^3
k	thermal conductivity, W/(m· ℃)	υ	kinematic viscosity, m^2/s
L	condensing surface length, m	ω	humidity ratio of mist air, kg/kg
m	air mass flow rate, kg/s		
n	number of channels	**Subscripts**	
P	water vapor pressure, Pa	a	moist air
q	total heat transfer rate, W/(kg·m^2)	v	water vapor
r	droplet radius, m	p	plate surface
R_g	specific ideal gas constant, J/(mol·K)	w	saturated water
s	channel gap, m	DW	dropwise
		FW	filmwise
Greek letters		in	inlet of air channel
α	surface inclination angle	out	outlet of air channel

1. Introduction

The air-conditioning in buildings consumes extensive energy and can be a heavy burden especially for buildings with large air change rate demand [1]. As a passive cooling solution, the indirect evaporative cooler (IEC) makes use of the water evaporative to cool the air by running only a small pump and fans [2]. In hot and humid areas, the IEC integrated with a central AC system can pre-handle the fresh air by recovering the cooling capacity of exhaust air [3]. Compared with current commonly adopted exhaust air energy recovery technologies, the IEC owns the advantages such as low cost, energy-efficient and free from cross-contamination [4]. In recent years, there is a great interest in developing the IEC with various configurations [5-7] and heat exchange materials [8-10] to enhance the cooling potentials for widespread application in hot and humid areas. This type of air treatment has gained fast development from a single field research discipline to a multidisciplinary research area, including thermodynamics, materials science, and mechanical engineering.

There are two distinct passages in the IEC, respectively designed for the primary air to be cooled and the secondary air that vaporizes the spraying water. Many research studies have focused on the surface wettability of secondary air channels in the IEC so as to improve the heat exchange efficiency that is dominated by the water film evaporation. Zhao et al. [8] compared the thermal conductivity and water-retaining capacity of different heat and mass exchanging materials of IEC, among which the heat transfer rate ranges between 392~399 W/m^2. The wick-attained aluminum sheet is the most preferable one for the advantages of easy shape formation, durability, low cost and compatibility with coatings. Guilizzoni et al. [11] evaluated the static contact angle and water retention of the IEC heat exchanger with two different surface coatings. According to the experimental results, the novel hydrophilic coating could

improve the wet-bulb effectiveness of IEC by up to 10% than the conventional epoxy coating. Wang [12] studied the effects of water-retention capacity on the cooling performance of IEC by measuring the receding contact angles of different aluminum surfaces. Results showed that the high wicking surfaces with reduced dynamic contact angles could dramatically increase the cooling effectiveness of the IEC, especially at a lower water flow rate. Xu et al. [13] investigated the properties of seven different wet channel surface mediums in an IEC. It is found that the wicking ability, diffusion ability and evaporation ability of the textile fabrics were more than 171%, 298%, 77% respectively higher than the Kraft paper. Joohyun and Dae-Young [14] fabricated and tested a novel regenerative IEC with hydrophilic coating on the internal surface of wet channels. Due to the improved surface wettability, the evenly distributed water film and higher cooling effectiveness can be obtained at a minimized water flow rate.

In the IEC hybrid AC system used for energy recovery in hot and humid areas, the fresh air in the dry channels can be cooled below its dew point to condense the moisture. Not only sensible cooling but also the dehumidification effect of the fresh air can be expected in the IEC unit due to the condensation that occurs. Chen et al. [15] established a one-dimensional counter-flow IEC model considering three different states: non-condensation, partial condensation and total condensation. Min et al. [16] numerically studied and compared the possibility of fresh air condensation occurrence and its impact on the performance of IEC with cross-flow and counter-flow configurations. Meng et al. [17] obtained the turning points of IEC from non-condensation to partial and full condensation states through a visualized experimental study. Wan et al. [18] developed a computational fluid dynamics (CFD) model of a counter-flow IEC to study the heat and mass transfer coefficients in the presence of condensation. They further proposed a novel dew-point IEC [19] which enables the dehumidification and addressed the effect of condensation by a mathematical model. Pandelidis et al. [20] performed a simulation study on the IEC operating as a total heat recovery device for reducing the AC energy requirement based on an analytical ε–NTU model [21]. As the plate materials of IEC heat exchangers are mostly naturally hydrophilic aluminum, previous studies are all focused on numerical models that simplified the primary air condensation as an evenly distributed water film. However, the enhanced measures for the heat and mass transfer process specifically tailored to the IEC with condensation deserve further investigation.

Over the past decade, the surface modification technology for heat exchangers with condensate retention has received considerable attention, especially in the AC industries. Wang et al. [22] fabricated a novel fin-tube heat exchanger with superhydrophobic foils. It can improve the cooling capacity of the air-conditioner by 8% higher than the conventional hydrophilic one. Rainieri et al. [23] estimated the saturated humid air condensation on vertically placed aluminum plates coated with a hydrophobic oleic film. The results showed an average increase of about 25% on the convective heat transfer coefficient compared to the uncoated case. Baojin et al. [24] employed visual experiments to investigate the steam condensation on vertical titanium plates. For the same subcooling temperature, the tested heat transfer

coefficient of the uncoated surface was higher than the surface with the hydrophilic coating but lower than the surface with hydrophobic coating. Rajkumar et al. [25] tested the performance of a lead coated copper tube that has a greater contact angle than the bare copper tube. A maximum enhancement of 115.8% for the overall heat transfer coefficient was achieved due to the accelerated removal of steam condensation. Table 1 summarized the relevant findings in the literature review of condensation heat transfer enhancement of AC applications associated with surface modification technologies.

Such observation suggested that the improved cooling capacity and dehumidification performance for the IEC heat exchangers could be attributed to the promotion of dropwise condensation on hydrophobic surfaces. In hot and humid areas, the IEC operates under partial or total condensation states for about half of the annual operation time, and the achieved latent cooling accounts for 41.3% of annual total cooling capacity [26]. Although the dehumidifying process contributes to the total heat transfer rate of the IEC, it degrades the sensible efficiency due to the condensate retention on the heat exchanger plates [27]. The aluminum sheets widely used for fabricating the IEC heat exchangers are naturally hydrophilic [28], which is not favorable for the condensate water drainage and therefore increases the heat transfer resistances. However, existing research on the surface modification of IEC has only focused on the surface wettability of wet channels for achieving a higher evaporation rate, the heat and mass transfer enhancements for the dry channels of IEC considering condensation was rarely addressed.

In view of the above, this study investigated the enhanced heat transfer performance of an IEC with hydrophobic coating for fresh air pre-handling in hot and humid areas. Firstly, a novel IEC heat exchanger was fabricated by depositing the hydrophobic nanoparticles on the surfaces of primary air channels. Microstructures of the bare and coated aluminum plate samples were identified using scanning electron microscopy (SEM) tests. Then, visual experiments were carried out to observe the primary air condensation (i.e. filmwise and dropwise mechanisms) on different plate surfaces. Besides, the droplet behaviors on the plate surfaces with and without hydrophobic coating were compared under both dynamic and steady states. Finally, the influence of operating conditions on the sensible cooling and dehumidifying performance subject to the surface properties have been thoroughly analyzed. The results of this study contribute to the IEC upgrading with more innovative surface treatments for offering better condensate drainage and improving the energy efficiency of AC systems.

Table 1 Previous studies concerning the effects of hydrophobic coatings on the performance of heat exchangers

No.	Researcher	Surface material	Coating	Fluid type	Sub-cooling temperature	Contact angle θ	Outcome
1	Baojin et al. [24]	Titanium plates	Titania nanorods [29]	Pure steam	2-22℃	θ = 100°	The hydrophobic surface achieves higher heat flux (0-10 W/m^2) than the hydrophilic one (0-3 W/m^2) for various sub-cooling temperature.
2	Rajkumar et al. [25]	Copper tubes with grooves	10 μm lead coating	Pure steam	0.5-20 ℃	θ = 114°	Lead coated copper tube with a groove depth of 0.1mm demonstrates the maximum condensation heat transfer coefficient (110.8 kW/m^2·K) than the bare copper tube (75.4 kW/m^2·K) at a low degree of sub-cooling (ΔT= 1.5 ℃).
3	Yang et al. [30]	Copper plates	Ethyl nonafluorobutyl ether	Moist air (40-85%)	10-18℃	θ = 125°	The heat transfer coefficient of moist air on the hydrophobic surface (20 – 29 W/m^2·K) can be 3-7% higher than the hydrophilic one.
4	Lara and Holtzapple [31]	Titanium plates	Ni–P–PTFE coating of 0.635-127 μm thickness	Saturated steam	0-1.4℃	-	The 2.54-μm-thick lead-containing Ni–P–PTFE hydrophobic coating deposited on the bare titanium plates can greatly improve the heat transfer coefficient from 78 kW/m^2·K to 240 kW/m^2·K.
5	Wang et al. [22]	Aluminum-foils	H,1H,2H,2H-perfluorodecyl-triethoxysilane	Moist air (75%)	13-18 ℃	θ = 160°	The cooling capacity of the super-hydrophobic heat exchanger is 8.06% higher than that of the hydrophilic exchangers.
6	Rainieri and Pagliarini [23]	3-mm thick aluminum plate	A thin oleic film	Saturated humid air	2.3-8.2℃	θ = 91°	The convective heat transfer coefficient of the coated surface (250-520 W/m^2·K) is increased by 25% compared to the uncoated case.
7	Torresin et al. [32]	Copper samples	H,1H,2H,2H-Perfluorodecanethiol	Saturated vapor at 110 ℃	2-16 ℃	θ = 159°	The super-hydrophobic sample can achieve higher heat flux (600 kW/m^2) than the oxidized copper sample (440 kW/m^2), especially at high sub-cooling temperature (10℃).
8	Hu et al. [33]	Metal Foam (copper)	$CuO/Cu(OH)_2$ micro/nanostructures	Moist air (27–35 ℃, 30-90%)	9-23 ℃	θ_{adv} = 161° θ_{rec} = 139°	The heat transfer coefficient on the metal foam with a hydrophobic coating (180-420 W/m^2·K) is 5–34% larger than that on uncoated metal foam under dehumidifying conditions.

2 Fabrication of IEC with a hydrophobic coating

To evaluate the surface energy on the overall heat transfer performance of primary air condensation, comparative experiments were conducted on both the conventional plate-type aluminum IEC and the one treated with silicon nanomaterials. Table 2 lists the specifications of the aluminum heat exchanger used in this study. The IEC heat exchanger with a hydrophobic coating on primary air channel surfaces was fabricated by following seven-step process as: (i) the heat exchanger with bare-aluminum plates was rinsed by acetone constantly for 5 min; (ii) spraying the deionized water to wash off the residual pollutants for 10 min, and dried; (iii) blocking materials were applied to the secondary air inlet and outlet of the heat exchanger to prevent the wet channel surfaces from contacting the coating; (iv) the hydrophobicity of primary air channels was rendered by immersing the heat exchanger in an aqueous solution of nanoparticles for 30 min to form a molecular structure consisting of (R2SiO)x on the plate surfaces; (v) the heat exchanger was baked in the oven at 50℃ by 1 h to improve the stability of nano-coating; (vi) thoroughly clean the heat exchanger by deionized water, and then dried. Fig. 1 shows the detailed fabrication process.

Table 2 Specifications of the IEC heat exchanger

Parameters	Value
Cooler length (L)	0.4 m
Cooler width (W)	0.2 m
Cooler height (H)	0.4 m
Channel gap (s)	4 mm
Number of channel pairs (n)	25
Aluminum plate thickness (δ)	0.15 mm

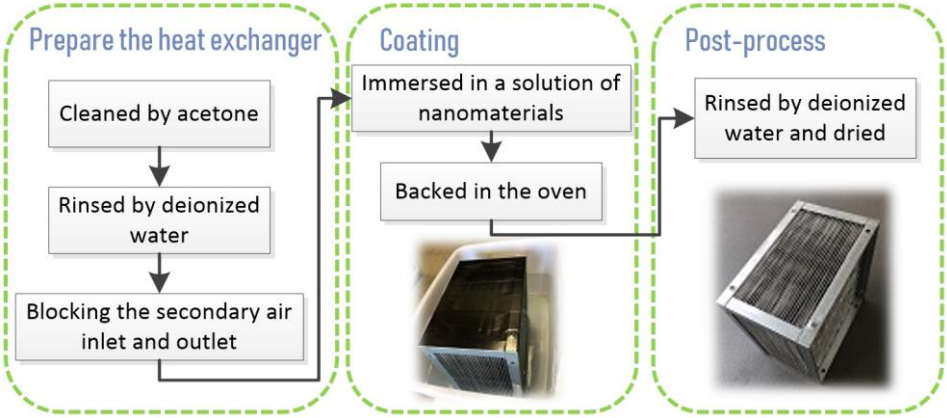

Fig. 1 Fabrication process of the IEC heat exchanger hydrophobic-coated primary air channels

2.1 Characterization of the hydrophobic coating

The IEC with hydrophobic primary air channels had been fabricated for observing the water condensing phenomenon and analyzing the heat and mass transfer performance. High-resolution scanning electron microscopy (SEM) tests were conducted to investigate the microscopic morphology of hydrophobic coating deposited on the surface. Fig. 2 shows SEM images of the bare aluminum plate surface and the coating surface morphology. It appears that the densely-distributed spherical protrusions exist on the modified surface and can produce countless voids for the droplets in contact with the surface. Therefore, the nanostructure can effectively avoid water film forming on the surface, granting the hydrophobic characteristic for heat exchange plates. The average coating thickness is about 5μm, which is much thinner than the thickness of the aluminum heat exchange plate (0.152 mm). As the thermal conductivity of hydrophobic coating is about 12.2 $W/m \cdot K^{-1}$[31], the resistance of the thin coating that has a weak impact on the overall thermal conductivity of heat exchanger plates was ignored [34].

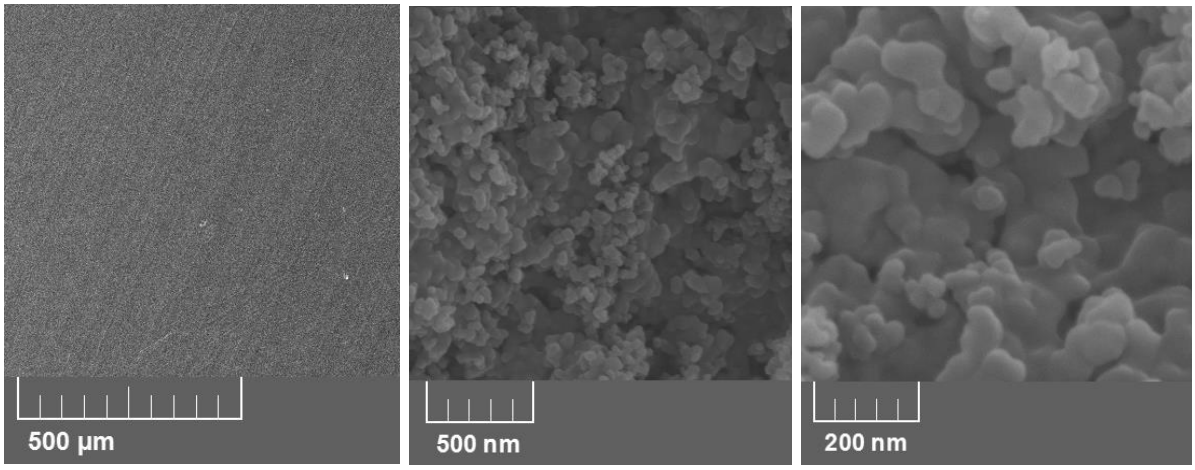

(a) bare aluminum surface (b) hydrophobic coating

Fig. 2 SEM images of plate surface and nanoparticles

2.2 Contact angle

The contact angle measurement is an effective method to characterize the overall wettability of a surface. In addition to the static contact angle, the dynamic contact angle is also commonly used for a surface to provide information about contact angle hysteresis. To measure the static and dynamic contact angles of the aluminum heat exchange plate, a contact angle meter (JCY20-13) was used. The contact angles of un-coated and hydrophobic sample plates were compared as Fig. 3a shows. For the static contact angle measured on the horizontal sample plate, a remarkable increase from 78° to 106° was observed on the plate surface after performing the hydrophobic coating. The contact angle hysteresis [25], defined as the difference between advancing and receding contact angles ($\theta_{adv} - \theta_{rec}$), reflects the surface adhesion for droplet movement [35]. For inclined surface on which the droplet starts to roll-off due to the gravity effect, the advancing and receding angles can be measured to calculate the contact angle hysteresis for each sample plate. Surfaces with low contact angle hysteresis generally retain less water

than those with high contact angle hysteresis. It is worth noting in Fig. 3b that the hydrophobic surface has a smaller contact angle hysteresis of 13° than the un-coated surface (16°), indicating the droplets can slide off from the hydrophobic surface more easily. The contact angles on the coated and uncoated aluminum plate surfaces are listed in Table 3.

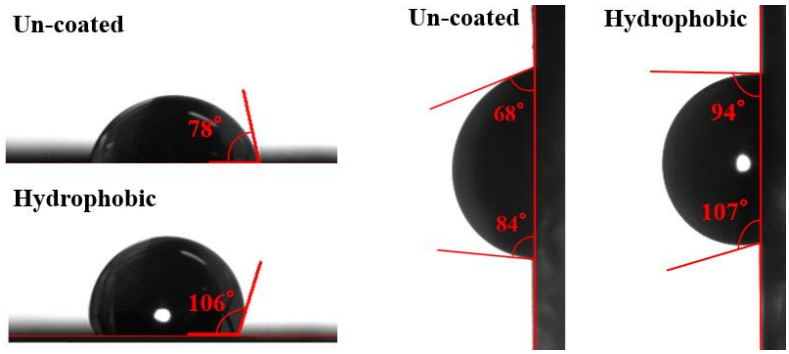

(a) Static contact angle (b) Advancing and receding contact angle

Fig. 3 Contact angles of different plate surfaces

Table 3 Contact angles of coated and uncoated aluminum plate surfaces

Sample	Static contact angle	Advancing contact angle θ_{adv}	Receding contact angle θ_{rec}	Contact angle hysteresis
Uncoated surface	78°	84°	68°	16°
Hydrophobic surface	106°	107°	94°	13°

3. Experimental setup and procedures

3.1 IEC test rig

Visual experiments were carried out on both the IEC heat exchangers with and without hydrophobic coating to investigate the effect of surface modification on the heat transfer characteristics of primary air under dehumidifying conditions. Fig. 4 and Fig. 5 show the schematic diagram and photo of a cross-flow IEC test rig which mainly consists of three main loops including primary air, secondary air and the spraying water. The primary air and secondary air both come from the air-conditioned space with stable indoor thermal conditions. A humidifier and a heater were installed in the primary air duct to produce the inlet air at a certain temperature and relative humidity. In an IEC, the core component is the heat exchanger which consists of alternative dry and wet channels. With a size of 0.4 m × 0.4 m, the heat exchanger plates are separated by the neatly arranged inward and outward small projections to form a channel gap of 4 mm for the air flows. As the cold and dry secondary air was utilized to evaporate the spraying water in the wet channels and take the heat away, the primary air in dry channels can be cooled by the plate surfaces to condense the moisture. As shown in Fig. 5, the outer primary air channel in the heat exchanger is covered with a transparent plate that allows the viewing of moist air condensation on

the heat exchanger plate. An extra glass cover was fixed outside the viewing window to form an air layer for thermal insulation. The polyurethane insulation was attached to the exterior of air ducts to prevent heat loss to the environment.

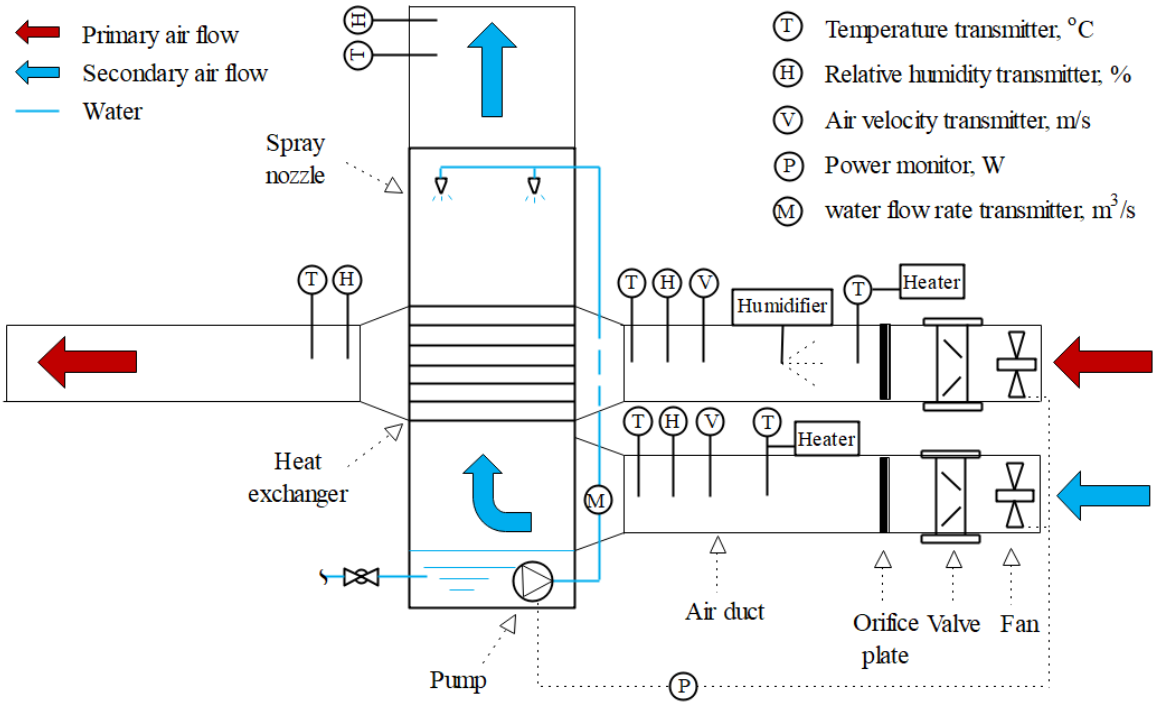

Fig. 4 Schematic of experimental apparatus

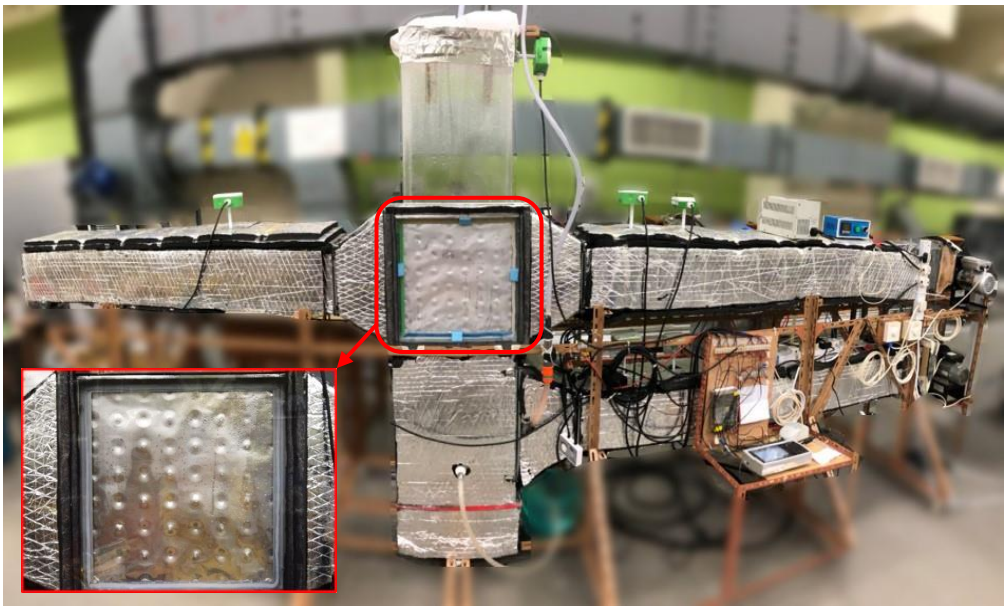

Fig. 5 Photo of the IEC test rig

After the primary air being adjusted to the required temperature and relative humidity conditions, it was provided to the heat exchanger for cooling and dehumidifying. The water vapor in moist air condenses on the cold surfaces, resulting in a successive process of nucleation, water droplet growth and ultimately fall-off. Along with the condensation accumulation, the heat and mass transfer in the IEC go through a dynamic evolution before reaching the steady-state. The condensation modes of primary air on the heat exchanger plates with and without hydrophobic coating present different characteristics in terms of both the dynamic and steady states. To capture the dynamic condensation behaviors, a high-speed CCD camera (Phantom, M-110 with Nikon, AF Micro Nikkor 60 mm lens) was placed in front of the chamber. The falling frequency of the droplets detached from the plate surface was measured using a stopwatch. Besides, the primary airflow rate, temperature and relative humidity at the inlet and outlet were measured by the sensors listed in Table 4. The data collection interval of the sensors was set at 2s.

Table 4 Specification of different measuring instruments

Parameters	Device	Range	Accuracy
Dry bulb temperature	Pt1000 Model: EE160	-15-60 ℃	±0.3 ℃
Relative humidity	Pt1000 Model: EE160	10-95% RH	±2.5% RH
Air velocity	Hot film anemometer Model: EE65	0-10 m/s	±0.2 m/s
Data logger	GRAPHTEC GL820, 12 channels		

3.2 Test conditions

Several test conditions have been conducted to evaluate the performance of coated and un-coated heat exchangers for the IEC under different dehumidifying conditions. As listed in Table 5, the primary air inlet states have been set in certain ranges to produce representative operating conditions with different outdoor temperatures, relative humidity and ratio of primary air to secondary air flow volume. For the IEC used as an energy recovery unit in the AC system, the secondary air is the exhaust air from controlled indoor spaces, which were stabilized at 24 ℃ and 60% in this study. Considering the effect of air velocity on the trade-off between heat transfer rate and air pressure drop, the air velocity can be set at an optimized value of 2.0 m/s. However, the ratio of primary air to secondary air flow volume can be varied from 1 under different application cases, such as cleam room provided with positive pressure to prevent contaminants entering and pollutant room with negative pressure. The steady-state for each test case is defined as the outlet air temperature and relative humidity variations are within 0.15 ℃ and 2% for 5 min.

Table 5 Settings of controllable parameters under various test conditions

Parameters	$t_{p,in}$ (℃)	$RH_{p,in}$ (%)	u_p/u_s

$t_{p,in}$	**[30, 32, 34, 36]**	80	80
$RH_{p,in}$	30	**[60, 70, 80, 90]**	30
u_p/u_s	1	1	**[0.5, 1, 1.5, 2]**

3.2.1 Performance indicators

For the plate-type IEC under dehumidifying conditions, heat and mass transfer occur in both the primary air and secondary air channels separated by the heat exchanger plates. Due to the much lower water vapor pressure of the saturated air at plate temperature, the primary air is cooled and condensates on the plate surface with latent heat transferred to the secondary air on the other side. To evaluate the cooling and dehumidifying performance of the IEC with coated and uncoated plate surfaces, two performance indexes, namely the wet-bulb efficiency and dehumidification efficiency were proposed.

The wet-bulb effectiveness (η_{wb}) evaluates the sensible cooling performance of IEC by describing the extent of the approach of outlet air temperature to the wet-bulb temperature of inlet secondary air ($t_{wb,s}$). It is expressed as Eq. (1).

$$\eta_{wb} = \frac{t_{p,in} - t_{p,out}}{t_{p,in} - t_{wb,s}} \tag{1}$$

Under the dehumidifying conditions, another evaluation index is needed to evaluate the performance of IEC in handling the latent heat. Therefore, the dehumidification efficiency (η_ω) is introduced as a ratio of the removed moisture of primary air to the moisture difference between the inlet primary air and saturated air at the wet-bulb temperature of inlet secondary air ($\omega_{t_{wb}}$), as shown in Eq. (2).

$$\eta_\omega = \frac{\omega_{p,in} - \omega_{p,out}}{\omega_{p,in} - \omega_{t_{wb}}} \tag{2}$$

To evaluate the energy-saving potential of the IEC under dehumidifying conditions, the energy recovery rate ($E_{recovery}$, kW/kg) was proposed, as calculated in Eq. (3). It is calculated as a ratio of total heat removed from primary air per mass unit to the overall coefficient of performance (COP), representing the energy-saving per unit time of a central AC system that coupled with an IEC unit in handling the pre-unit mass of fresh air.

$$E_{recovery} = \frac{Q_{recovery}}{m_a COP} = \frac{\eta_{wb} c_{pa}\left(t_{p,in} - t_{wb,s}\right) + \eta_\omega h_{fg}\left(\omega_{p,in} - \omega_{t_{wb}}\right)}{COP} \tag{3}$$

where, $Q_{recovery}$ is the achieved total heat recovery of IEC by capturing the cooling potential of the secondary air, kW; the COP in this study is set as 2.5 according to the conventional central cooling systems in the market [36].

The falling droplet mass and falling frequency are the two key indicators to evaluate the surface properties for condensate formation and drainage. When the condensation of primary air starts, the

droplets nucleate on the plate surfaces of IEC, and grow into larger ones over time through continuous vapor condensation and droplet coalescence. The maximum size of a droplet attached on the vertical surface before drained by gravity depends on the surface tension forces that vary with the contact angle hysteresis. A theoretical equation developed by Sugawara and Michiyoshi [37] can be used to calculate the droplet departure diameter (D_d), as expressed in Eq. (4). The falling droplet mass (M_d, mg) can be derived using the two-circle method proposed by Elsherbini and Jacobi [38], as expressed in Eq. (5).

$$D_d = \left[\left(\frac{\sigma_l}{\rho_l g}\right) \cdot \left(\frac{16sin^3\theta_M}{2\theta_M - \sin(2\theta_M)}\right) \cdot sin\left(\frac{\theta_{adv} - \theta_{rec}}{2}\right)\right]^{\frac{1}{2}} \tag{4}$$

$$M_d = \rho_l \int_0^{2\pi} f(D_d, \theta_{adv}, \theta_{rec}) d\phi \tag{5}$$

where, σ_l is the water surface tension which is set to be 73.7×10^{-3} N/m, ρ_l is the liquid density which regards as 998 kg/m^3, θ_M is the mean contact angle ($\theta_M = (\theta_{adv} + \theta_{rec})/2$) of the surface.

In this study, the droplet departure sizes on the plate surfaces with and without hydrophobic coating were theoretically calculated respectively and compared to the tested droplet profiles which are observed during the experiments and processed by an image processing method [27]. Meanwhile, the real-time droplet falling frequency (f_d) for the steady-state conditions of IEC was measured using a stopwatch.

3.2.2 Uncertainty analysis

Due to the uncertainties associated with the measurements, the validation of experimental results should be performed for all the variables. The uncertainty concerning performance indicators was attained by combining the effects of systematic uncertainty for each test parameter according to the reference [39]. Fig. 6 presents the profiles of inlet primary air temperature and relative humidity during the test duration under different experimental conditions. It can be seen that the inlet air temperature and humidity could reach the set values after turning on the system for several minutes. Therefore, the timing for condensation evolution in IEC should be started after the inlet air parameters reaching the pre-set values. The whole tests last for 3 hours in order to cover the dynamic evolution of primary air condensation until the steady-state operating conditions were achieved.

Table 6 Uncertainty analysis results

Parameter	Unit	Nominal value		Uncertainty	
		Coated IEC	Uncoated IEC	Coated IEC	Uncoated IEC
$t_{p,out}$	℃	23.2	23.6	±1.4%	±1.7%
$RH_{p,out}$	%	17.0	17.6	±2.8%	±3.1%
M_d	mg	38.7	57.2	±13.8%	±16.0%
f_d	Hz	0.40	0.24	±16.4%	±19.0%

η_{wb}	-	0.63	0.57	±4.6%	±5.1%
η_{ω}	-	0.57	0.48	±5.9%	±7.5%
$E_{recovery}$	kW/kg	7.79	6.89	±8.9%	±10.7%

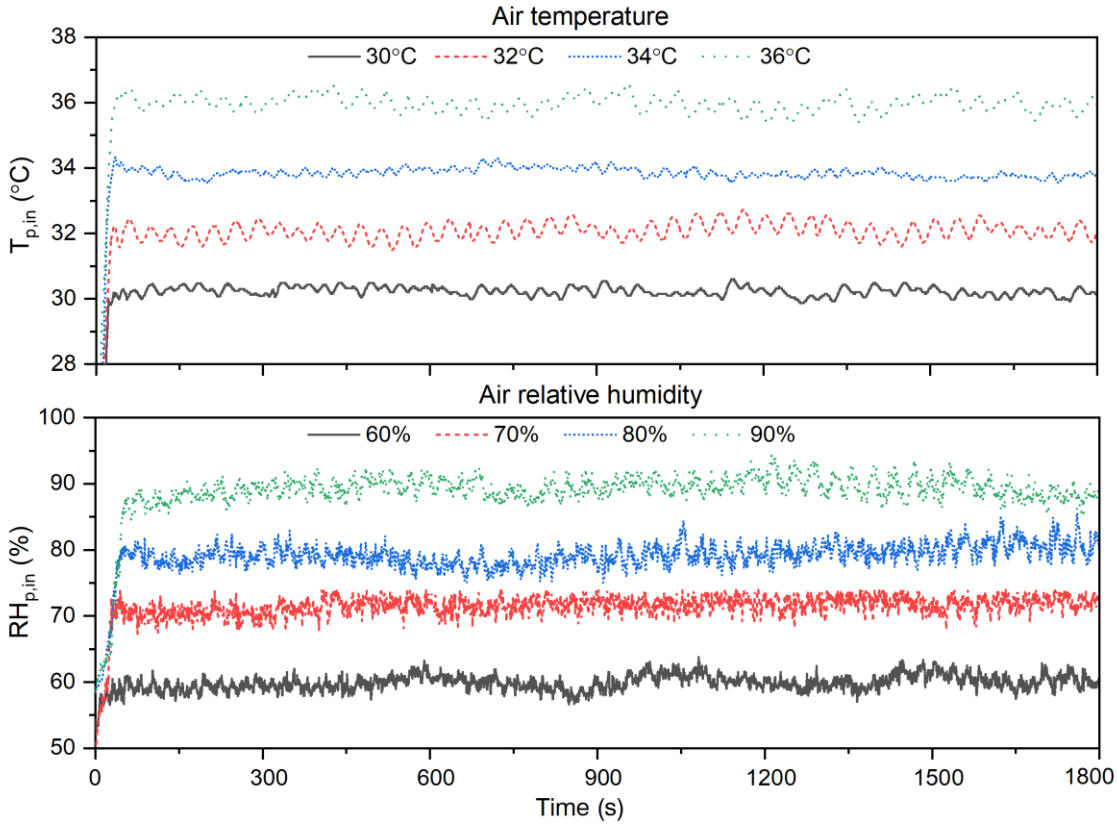

Fig. 6 Profiles of inlet primary air temperature and relative humidity during the test duration

The uncertainty analysis results of the performance indicators under steady-state conditions are listed in Table 6. For the observed condensate droplet profiles such as falling frequency (f_d) and departure diameter (D_d), the uncertainties are derived from the results of multiple measurements during the tests. In fact, as the experimental conditions and apparatus are unchanged for controlled experiments on both the IECs with and without hydrophobic coating, the relatively high uncertainties of the test variables under dynamic conditions could not invalidate the performance comparison results [23].

4. Results and discussion

By combining the visualized observation and measured data, the performance comparison between the IEC with and without hydrophobic coating under dehumidifying conditions was conducted in this section. Specifically, the condensation mechanism on heat exchanger plates with different surface properties and its effects on the dynamic performance of IEC was investigated through a case study. Moreover, based on the measured results under different inlet air temperature and relative humidity, the steady-state sensible cooling and dehumidifying performance were compared between the coated and uncoated IEC. Their differences in the energy-saving potential were also analyzed.

4.1 Condensation mode

The condensate evolution on the bare and hydrophobic plate surfaces and its effects on the dynamic operating performance of the IEC was studied through experimental analysis of a case study ($t_p = 30℃, RH_p = 82\%, u_p = 2m/s, t_s = 24℃, RH_s = 65\%, u_s = 2m/s$). From the initial starting of the test to the steady-state operation mode, the variations on outlet air temperature and relative humidity from the two heat exchangers were plotted. Moreover, the visual observations of condensation growth and the steady-state condensation characteristics (i.e. droplet falling frequency, droplet departure size) were compared between the IECs with and without hydrophobic coating.

4.1.1 Dynamic performance of IEC

Fig. 7 presents the outlet primary air temperature and humidity variations after starting up the systems for coated and uncoated IECs. It can be seen that the outlet air humidity of the two systems both increase sharply in the first 150s as soon as the humidifier is turned on, followed by a slow climb before reaching the steady-state. Due to the effect of condensation growth that degrades the heat transfer performance, the steady-state outlet temperatures of the two IECs are both higher than the initial values when the primary air flowing over the dry surfaces. However, the two IECs differed in the time durations for condensation evolution as well as the outlet air statuses under steady-state operating conditions. It takes 750s for the condensation growth on plate surfaces of the un-coated IEC to attain a balance between the deposition and shedding when the outlet air state is maintained at 23.6 ℃ and 17.6 g/kg. For the IEC with a hydrophobic coating, the steady-state with stable dropwise condensation can be reached shortly after 400s. Compared to the un-coated IEC, the heat transfer degradation resulting from the dynamic condensation evolution is slighter on the coated surfaces, and the primary air can be processed to a lower outlet temperature of 23.2 ℃ with less moisture content of 17.0 g/kg.

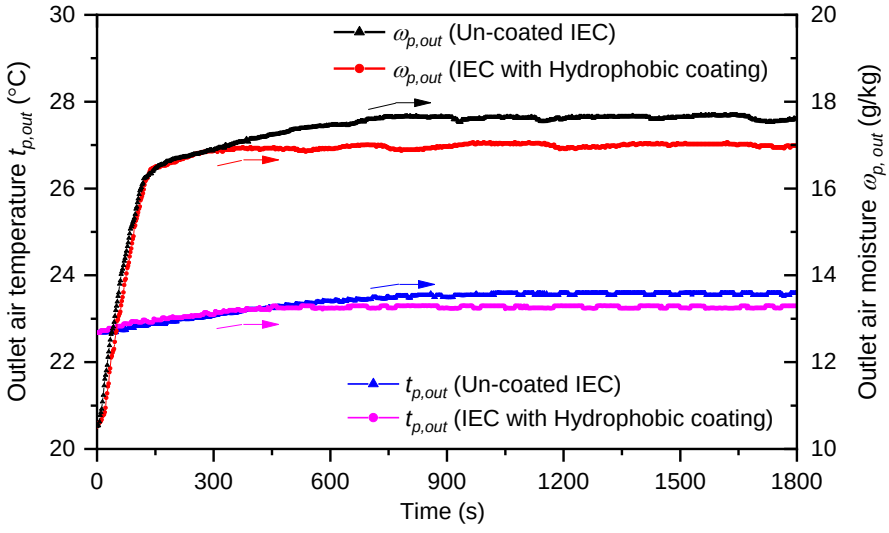

Fig. 7 Comparisons on the outlet air variation process of coated and un-coated IEC

4.1.2 Condensation growth

Fig. 8 demonstrates the different condensation mechanisms on the plate surfaces with and without hydrophobic coating. Four stages during the condensation growth from initial nucleation (I), growth (II), coalescence (III) and eventual departure (IV) were identified for each surface. The condensation growth on the uncoated surface took 13 minutes before reaching the steady-state operation with a dynamic equilibrium between condensate retention and drainage. By contrast, condensation on the hydrophobic surface grows rapidly from stage I to stage IV in 7 minutes.

It reveals that the condensation on bare-aluminum surface forms as large irregular droplets stuck on the surface and ultimately drained off as filmwise. The uncoated plate surface covered with condensate liquid film is associated with higher thermal resistance, suppressing the heat transfer performance of IEC under dehumidifying conditions. Due to the larger contact angle, condensation on the surface with hydrophobic coating forms as numerous spherical droplets by occupying fewer plate spaces and enlarging the heat transfer area in direct contact with the primary air. A smaller maximum volume was observed for the dropwise condensation on the coated surface when it is going to roll down by gravity. The falling droplets can sweep the surface and leave a refreshed nucleation site for new droplets to grow.

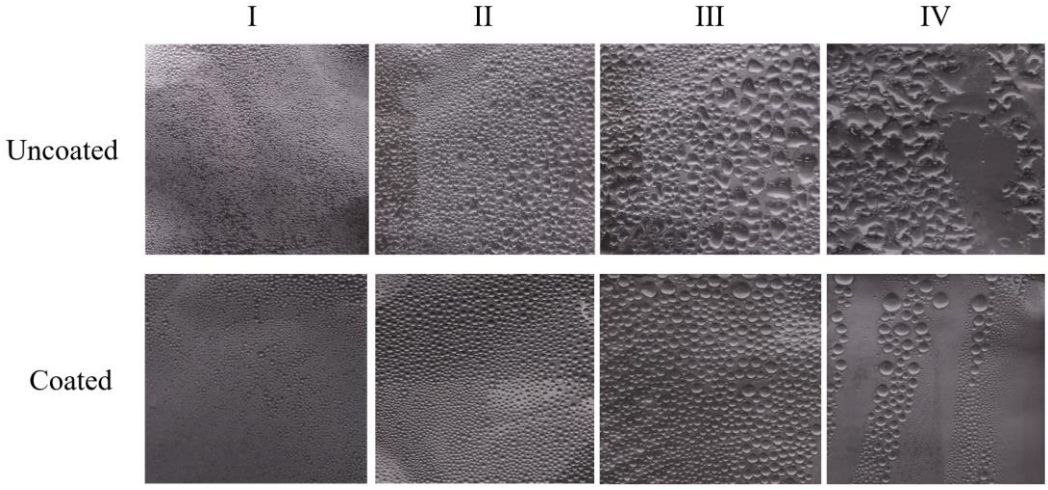

Fig. 8 Images of condensation on the plate surfaces of coated and uncoated IEC
(I: nucleation, II: growth, III: coalescence, IV: departure)

After the steady-state is attained for the system's operation, the average falling droplet mass and frequency on the two kinds of plate surfaces of IEC were collected, as plotted in Fig. 9. It can be seen that the hydrophobic plate surface exhibits a greater falling frequency and a smaller falling droplet mass compared to the uncoated one. The observed departure diameter of droplets adhered on the plate surfaces is 2-3 mm for the hydrophobic one and 4-6 mm for the bare-aluminum one, respectively. As the small droplets transfer heat more efficiently than the large ones, the hydrophobic surface of IEC can provide enhanced condensate heat transfer performance by enabling the droplet departure to happen at a smaller

size. Furthermore, the higher falling frequency on the hydrophobic surface (0.40 Hz) than on the uncoated surface (0.24 Hz) indicates more frequent periodical surface refreshment for contacting with air directly and allowing new drops to grow. The average falling droplet mass derived from experimental results are 38.7 mg for coated surface and 58.2 mg for uncoated plates, which are conformed to the calculated values based on theoretical maximum diameters.

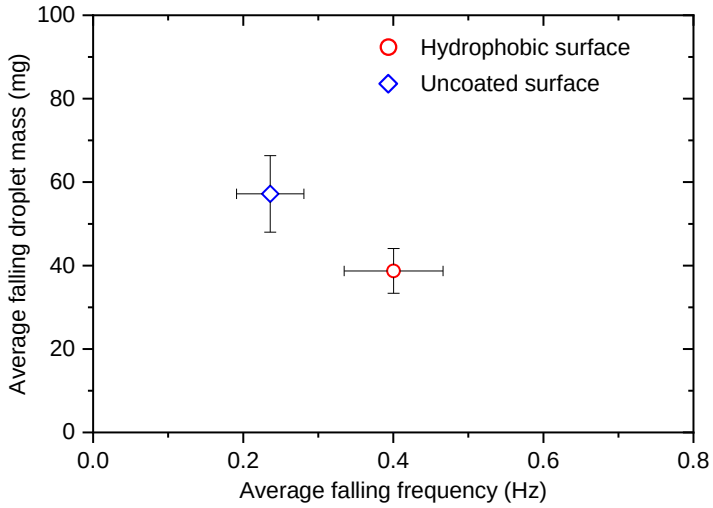

Fig. 9 Steady-state average falling mass and frequency of droplets on the plate surfaces

4.2 Sensible cooling and dehumidifying performance

In this part, the steady-state operating data of 7 cases under different inlet air conditions were selected to investigate the performance enhancement of IEC with a hydrophobic coating. The detailed information of each experimental condition was listed in Table 7. It is reported that the primary air inlet states have been set in order to produce representative operating conditions for IECs used as energy recovery units in hot and humid areas. For each case under the dehumidifying conditions, the outlet air temperature and moisture content of the coated IEC were all lower than those of the uncoated one. The comparisons on sensible cooling and dehumidification effectiveness between the IECs with and without hydrophobic coating were analyzed in the following subsections.

Table 7 Test results of coated and un-coated IEC under different experimental conditions

No.	Un-coated IEC				Coated IEC			
	$t_{p,in}$ (℃)	$\omega_{p,in}$ (g/kg)	$t_{p,out}$ (℃)	$\omega_{p,out}$ (g/kg)	$t_{p,in}$ (℃)	$\omega_{p,in}$ (g/kg)	$t_{p,out}$ (℃)	$\omega_{p,out}$ (g/kg)
1	30.09	21.43	23.60	17.60	30.13	22.08	23.36	17.00
2	31.56	23.49	24.23	18.40	32.08	24.18	24.21	18.41
3	33.92	26.43	25.75	19.62	33.80	26.83	25.09	19.37
4	35.62	29.27	27.17	20.68	35.83	30.00	25.90	20.27
5	30.18	16.60	22.19	15.71	30.15	61.18	21.92	15.21
6	30.34	19.29	22.72	16.92	30.22	71.87	22.55	16.42

7	30.19	24.60	24.71	18.66	30.16	90.71	24.04	17.82

4.2.1 Effect of inlet temperature

As the degree of sub-cooling increases with the rising inlet air temperature, a greater mass flow of condensate occurred on the plate surfaces, resulting in a decrease in wet-bulb effectiveness (η_{wb}) and an increase of dehumidification effectiveness (η_{ω}) for both of the two IECs. In Fig. 10, it is shown that the coated IEC provides a higher η_{wb} by 11.8% and higher η_{ω} by 13.1% on average than the un-coated one. With the inlet air temperature increases from 30 ℃ to 36 ℃, the degradation on η_{wb} of un-coated IEC is more than twice of the coated IEC due to the enlarged condensation area on the plate surfaces covered by liquid film. The hydrophobic plate surfaces contribute to smaller droplet departure size and shorter life cycle of dropwise condensation, which reduces the fluctuations in heat transfer and lowers the uncertainty bars of η_{wb} and η_{ω}.

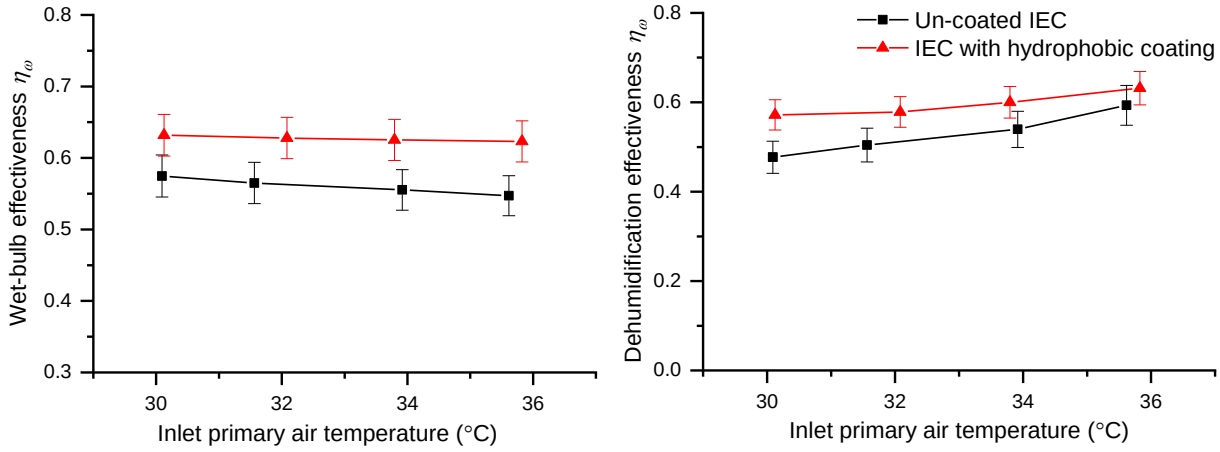

(a) Sensible cooling performance (b) dehumidifying performance

Fig.10 Performance of uncoated and coated IEC under different inlet air temperatures

4.2.2 Effect of inlet relative humidity

Fig. 11 presents the variation trend of η_{wb} and η_{ω} along with the increase of inlet relative humidity, which is consistent between the two IECs. With the inlet air relative humidity increases from 60% to 90%, the decline on η_{wb} of the uncoated IEC is more significant (from 0.68 to 0.50) than the coated one (from 0.70 to 0.60). The decrease in η_{wb} of the conventional uncoated IEC is more sensitive to the increasing inlet air humidity, since the condensate film expands on the surface that remarkably increases the heat transfer resistances. When the inlet air relative humidity is 60%, the dehumidification effectiveness (η_{ω}) of the coated IEC is twice as much as that of the uncoated one. While the η_{ω} is enhanced by only about 12.4% for the coated IEC under a higher inlet air humidity of 90%. Due to the excessive condensate water extracted from the highly humid air, the rivulet appears increasingly on both the uncoated and coated plate surfaces, breaking the direct contacts between moist air and plate surfaces.

Therefore, resulting from the decrease of dropwise nucleation sites, the improvement on η_ω is weakened under operating conditions with high inlet air humidity.

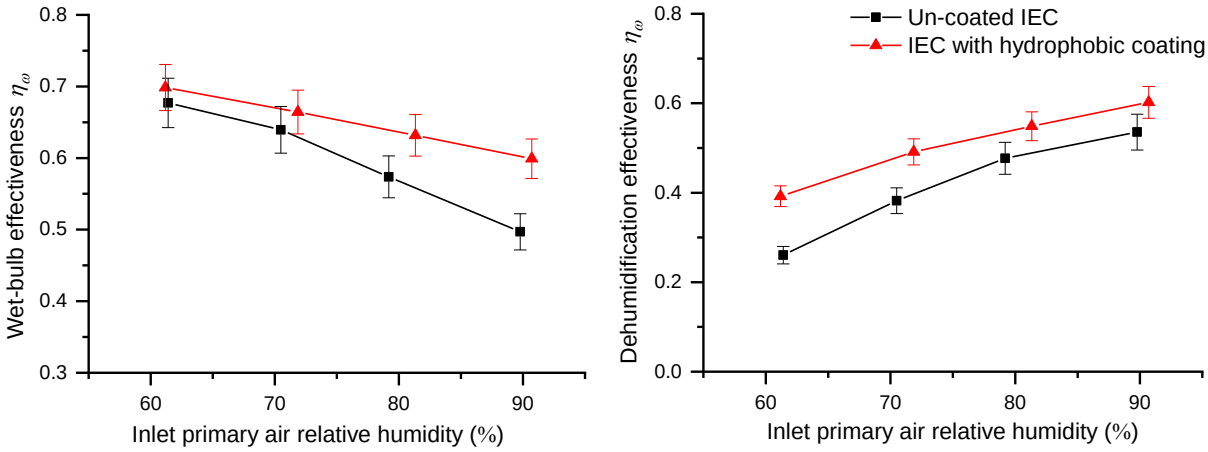

(a) Sensible cooling performance (b) dehumidifying performance

Fig. 11 Performance of uncoated and coated IEC under different inlet air relative humidity

4.3 Energy saving potential

To further estimate the effect of hydrophobic coating on energy saving potential, both the sensible and latent cooling performance was considered to compare the total energy recovery rates of IECs with coated and uncoated heat exchange plates. Fig. 12 shows the $E_{recovery}$ based on experimental results of two IECs under different inlet air conditions. It can be seen that the increases of inlet air temperature and relative humidity both result in approximately linear growths of the energy recovery rates for the two IECs, while the IEC with hydrophobic coating performs better than the uncoated one. Under all the tested conditions, the energy recovery rate of coated IEC is at an average of 14.1% higher than that of uncoated IEC. As the difference in condensation mechanisms subjected to surface properties becomes more pronounced with the rise of inlet air temperature and humidity, the coated IEC shows an increasing improvement on $E_{recovery}$ which varies from 8.5% to 17.2%.

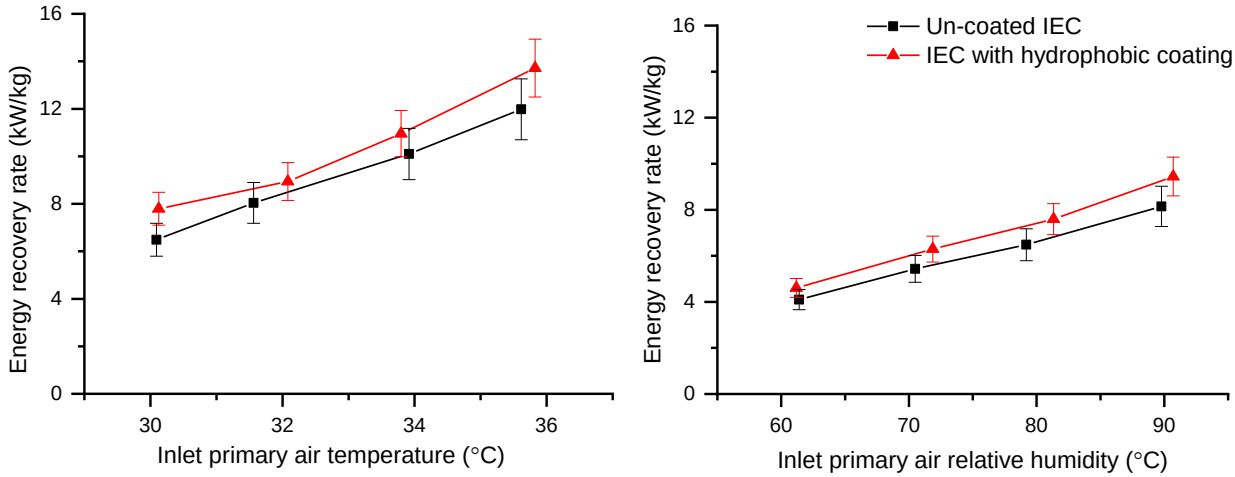

(a) different inlet air temperature (b) different inlet air relative humidity

Fig. 12 Energy recovery rate of uncoated and coated IEC

4.4 Sensitivity analysis

To obtain the importance of each inlet air parameters on the IEC performance with hydrophobic-coated channels, the sensitivity analysis was conducted using the orthogonal test. The experimental data of the un-coated IEC were also analyzed to derive the sensitivity which serves as a comparison group. In order to display the influence of inlet factors on the evaluation index, the factors - index trends are presented in Fig. 13 by using range method [40]. In terms of the wet-bulb effectiveness, the rank of influence for three parameters of the hydrophobic-coated IEC is: $RH_p > u_p/u_s > t_p$, while for un-coated IEC is: $u_p/u_s > RH_p > t_p$. It can be inferred from the results on section 4.2.2 that the IEC with hydrophobic channels could maintain a high wet-bulb effectiveness with the inceasing RH_p. For the dehumidification effectivess, the rank of influence for the two coolers coincides: $RH_p > u_p/u_s > t_p$. As for the energy recovery rate, the most influencial factor for hydrophobic-coated IEC is RH_p. While the energy recovery rate of un-coated IEC is more sensitive to air velocity ratio (u_p/u_s).

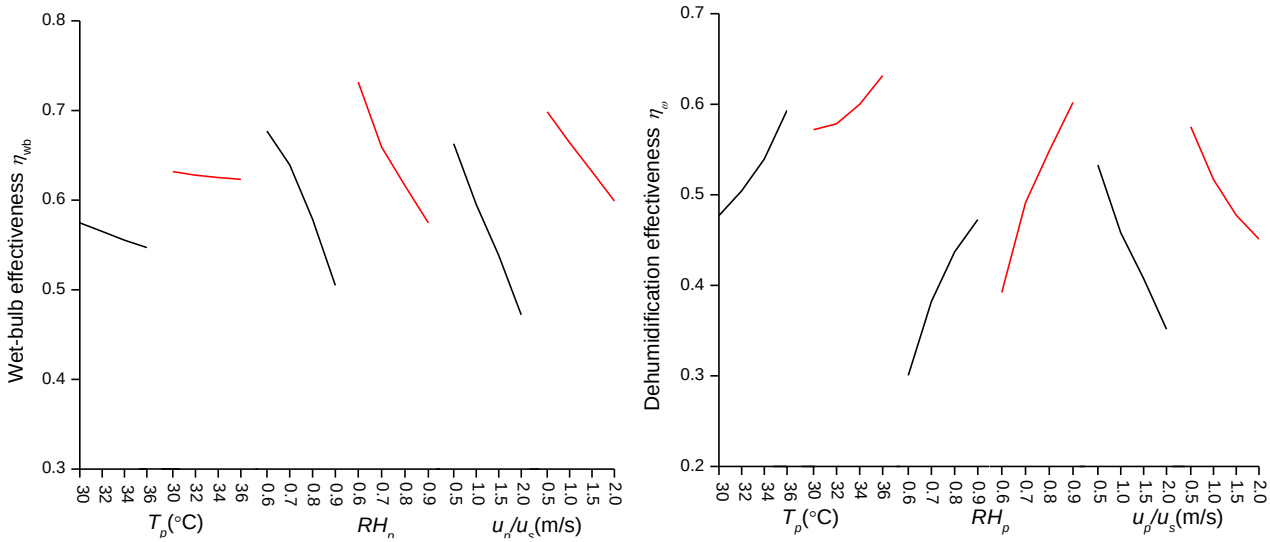

(a) Factors − wet-bulb effectiveness trend (b) Factors − dehumidification effectiveness trend

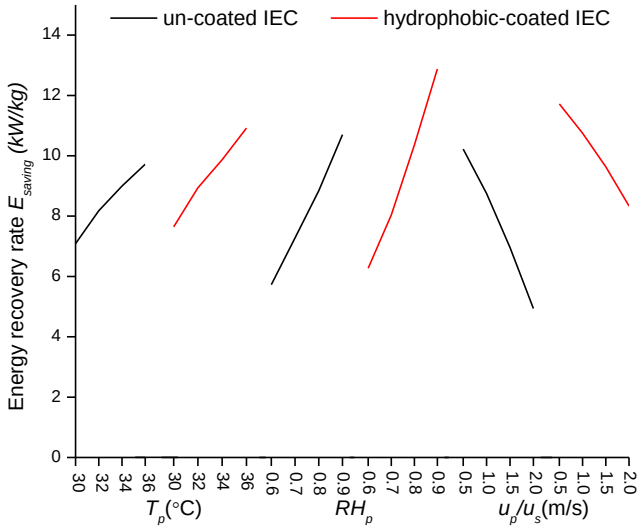

(c) Factors − energy recovery rate trend

Fig. 13 Factors –index trend

5. Conclusions

Potential energy savings of the central air-conditioning systems can be induced by the indirect evaporative cooler (IEC) through energy recovery from exhaust air to the fresh air. However, the condensation in the dry channels can pose significant influences on cooling performance, especially for the IEC used in hot and humid areas. In this paper, comparative experiments were carried out to estimate the effect of hydrophobic coating on the cooling performance and energy-saving potential of IEC under dehumidifying conditions. Such observations suggested that using hydrophobic coating materials on primary air channel surfaces of the IEC can potentially improve the energy recovery of AC systems in hot and humid areas. The main conclusions can be drawn as follows:

- From the visualized observation of the condensation mechanisms on heat exchange plates, the hydrophobic coating produces a higher contact angle for the plate surface, causing a reduced size of falling-off droplets and frequent droplet removal. The hydrophobic surface promotes dropwise condensation with a smaller droplet departure diameter of 2-3 mm, differed from the irregular droplets (4-6 mm) stuck on the bare-aluminum plate and drained off as filmwise.
- After starting up the experiments, the condensation accumulates on the plate surfaces, resulting in the deterioration of the heat transfer performance. The condensation on coated plate surfaces grows more quickly (400 seconds) than the uncoated surfaces (750 seconds) to attain a balance between the condensate deposition and shedding. The rapidly formed dropwise condensation on the hydrophobic surface has less deterioration effect on the convective heat transfer of primary air flowing over the heat exchange plates.

- Based on the measured data of processed air, the IEC with hydrophobic coating shows improved sensible cooling and dehumidifying performance for handling the fresh air due to more effective condensate drainage ability. The coated IEC provides higher wet-bulb effectiveness (η_{wb}) by 11.8% and higher dehumidification effectiveness (η_{ω}) by 13.1% at average than the un-coated one. The energy recovery rate ($E_{recovery}$) of coated IEC can be enhanced by 8.5-17.2% under various inlet air conditions.

CRediT authorship contribution statement

Yunran Min: Conceptualization, Methodology, Software, Writing - original draft. Wenchao Shi: Validation, Data curation. Boxu Shen: Resources, Formal analysis. Yi Chen: Investigation, Writing review & editing. Hongxing Yang: Supervision, Writing - review & editing.

ACKNOWLEDGEMENT

The work described in this paper was financially supported by the GRF research projects (No. 15213219 and No. 15200420) of the Research Grants Committee, the Hong Kong SAR Government.

REFERENCES

[1] C. Zhuang, K. Shan, S. Wang, Coordinated demand-controlled ventilation strategy for energy-efficient operation in multi-zone cleanroom air-conditioning systems, Building and Environment, 191 (2021) 107588.
[2] Y. Wan, J. Lin, K.J. Chua, C. Ren, A new method for prediction and analysis of heat and mass transfer in the counter-flow dew point evaporative cooler under diverse climatic, operating and geometric conditions, International Journal of Heat and Mass Transfer, 127 (2018) 1147-1160.
[3] W.-Y. Li, Y.-C. Li, L.-y. Zeng, J. Lu, Comparative study of vertical and horizontal indirect evaporative cooling heat recovery exchangers, International Journal of Heat and Mass Transfer, 124 (2018) 1245-1261.
[4] D. Pandelidis, A. Cichoń, A. Pacak, S. Anisimov, P. Drąg, Application of the cross-flow Maisotsenko cycle heat and mass exchanger to the moderate climate in different configurations in air-conditioning systems, International Journal of Heat and Mass Transfer, 122 (2018) 806-817.
[5] D. Pandelidis, S. Anisimov, W.M. Worek, Performance study of the Maisotsenko Cycle heat exchangers in different air-conditioning applications, International Journal of Heat and Mass Transfer, 81 (2015) 207-221.
[6] X. Cui, K.J. Chua, M.R. Islam, K.C. Ng, Performance evaluation of an indirect pre-cooling evaporative heat exchanger operating in hot and humid climate, Energy Conversion and Management, 102 (2015) 140-150.

[7] A.E. Kabeel, M. Abdelgaied, Numerical and experimental investigation of a novel configuration of indirect evaporative cooler with internal baffles, Energy Conversion and Management, 126 (2016) 526-536.
[8] X. Zhao, S. Liu, S. Riffat, Comparative study of heat and mass exchanging materials for indirect evaporative cooling systems, Building and Environment, 43(11) (2008) 1902-1911.
[9] F.J. Rey Martínez, E. Velasco Gómez, R. Herrero Martín, J. Martínez Gutiérrez, F. Varela Diez, Comparative study of two different evaporative systems: an indirect evaporative cooler and a semi-indirect ceramic evaporative cooler, Energy and Buildings, 36(7) (2004) 696-708.
[10] S. De Antonellis, L. Cignatta, C. Facchini, P. Liberati, Effect of heat exchanger plates geometry on performance of an indirect evaporative cooling system, Applied Thermal Engineering, 173 (2020) 115200.
[11] M. Guilizzoni, S. Milani, P. Liberati, S. De Antonellis, Effect of plates coating on performance of an indirect evaporative cooling system, International Journal of Refrigeration, 104 (2019) 367-375.
[12] T.A. Wang, R.L. Reid, Ashrae, Surface wettability effect on an indirect evaporative cooling system, Ashrae Transactions 1996, Vol 102, Pt 1, 102 (1996) 427-433.
[13] P. Xu, X. Ma, X. Zhao, K.S. Fancey, Experimental investigation on performance of fabrics for indirect evaporative cooling applications, Building and Environment, 110 (2016) 104-114.
[14] J. Lee, D.-Y. Lee, Experimental study of a counter flow regenerative evaporative cooler with finned channels, International Journal of Heat and Mass Transfer, 65 (2013) 173-179.
[15] Y. Chen, Y. Luo, H. Yang, A simplified analytical model for indirect evaporative cooling considering condensation from fresh air: Development and application, Energy and Buildings, 108 (2015) 387-400.
[16] Y. Min, Y. Chen, H. Yang, Numerical study on indirect evaporative coolers considering condensation: A thorough comparison between cross flow and counter flow, International Journal of Heat and Mass Transfer, 131 (2019) 472-486.
[17] D. Meng, J. Lv, Y. Chen, H. Li, X. Ma, Visualized experimental investigation on cross-flow indirect evaporative cooler with condensation, Applied Thermal Engineering, 145 (2018) 165-173.
[18] Y. Wan, A. Soh, Y. Shao, X. Cui, Y. Tang, K.J. Chua, Numerical study and correlations for heat and mass transfer coefficients in indirect evaporative coolers with condensation based on orthogonal test and CFD approach, International Journal of Heat and Mass Transfer, 153 (2020) 119580.
[19] Y. Wan, Z. Huang, A. Soh, X. Cui, K.J. Chua, Analysing the transport phenomena of novel dew-point evaporative coolers with different flow configurations considering condensation, International Journal of Heat and Mass Transfer, 170 (2021) 120991.
[20] D. Pandelidis, A. Cichoń, A. Pacak, S. Anisimov, P. Drąg, Counter-flow indirect evaporative cooler for heat recovery in the temperate climate, Energy, 165 (2018) 877-894.
[21] D. Pandelidis, A. Cichoń, A. Pacak, S. Anisimov, P. Drąg, Performance comparison between counter- and cross-flow indirect evaporative coolers for heat recovery in air conditioning systems in the presence of condensation in the product air channels, International Journal of Heat and Mass Transfer, 130 (2019) 757-777.
[22] S. Wang, X. Yu, C. Liang, Y. Zhang, Enhanced condensation heat transfer in air-conditioner heat exchanger using superhydrophobic foils, Applied Thermal Engineering, 137 (2018) 758-766.
[23] S. Rainieri, F. Bozzoli, G. Pagliarini, Effect of a hydrophobic coating on the local heat transfer coefficient in forced convection under wet conditions, Experimental heat transfer, 22(3) (2009) 163-177.

[24] Q. Baojin, Z. Li, X. Hong, S. Yan, Experimental study on condensation heat transfer of steam on vertical titanium plates with different surface energies, Experimental thermal and fluid science, 35(1) (2011) 211-218.
[25] M.R. Rajkumar, A. Praveen, R.A. Krishnan, L.G. Asirvatham, S. Wongwises, Experimental study of condensation heat transfer on hydrophobic vertical tube, International Journal of Heat and Mass Transfer, 120 (2018) 305-315.
[26] Y. Min, Y. Chen, H. Yang, A statistical modeling approach on the performance prediction of indirect evaporative cooling energy recovery systems, Applied Energy, 255 (2019) 113832.
[27] Y. Min, Y. Chen, H. Yang, C. Guo, Characteristics of primary air condensation in indirect evaporative cooler: Theoretical analysis and visualized validation, Building and Environment, (2020) 106783.
[28] M. Edalatpour, L. Liu, A.M. Jacobi, K. Eid, A. Sommers, Managing water on heat transfer surfaces: A critical review of techniques to modify surface wettability for applications with condensation or evaporation, Applied Energy, 222 (2018) 967-992.
[29] J.-M. Wu, Low-temperature preparation of titania nanorods through direct oxidation of titanium with hydrogen peroxide, Journal of crystal growth, 269(2-4) (2004) 347-355.
[30] K.-S. Yang, K.-H. Lin, C.-W. Tu, Y.-Z. He, C.-C. Wang, Experimental investigation of moist air condensation on hydrophilic, hydrophobic, superhydrophilic, and hybrid hydrophobic-hydrophilic surfaces, International Journal of Heat and Mass Transfer, 115 (2017) 1032-1041.
[31] J.R. Lara, M.T. Holtzapple, Experimental investigation of dropwise condensation on hydrophobic heat exchangers. Part II: Effect of coatings and surface geometry, Desalination, 280(1-3) (2011) 363-369.
[32] D. Torresin, M.K. Tiwari, D. Del Col, D. Poulikakos, Flow condensation on copper-based nanotextured superhydrophobic surfaces, Langmuir, 29(2) (2013) 840-848.
[33] H. Hu, Z. Lai, G. Ding, Heat transfer and pressure drop characteristics of wet air flow in metal foam with hydrophobic coating under dehumidifying conditions, Applied Thermal Engineering, 132 (2018) 651-664.
[34] C. Dong, L. Lu, T. Wen, Experimental study on dehumidification performance enhancement by TiO2 superhydrophilic coating for liquid desiccant plate dehumidifiers, Building and Environment, 124 (2017) 219-231.
[35] K. Rykaczewski, Microdroplet Growth Mechanism during Water Condensation on Superhydrophobic Surfaces, Langmuir, 28(20) (2012) 7720-7729.
[36] C. Zhuang, S. Wang, K. Shan, Adaptive full-range decoupled ventilation strategy and air-conditioning systems for cleanrooms and buildings requiring strict humidity control and their performance evaluation, Energy, 168 (2019) 883-896.
[37] S. Sugawara, I. Michiyoshi, Dropwise condensation, Mem. Fac. Engng, Kyoto Univ, 18(0.2) (1956).
[38] A.I. ElSherbini, A.M. Jacobi, A Model for Condensate Retention on Plain-Fin Heat Exchangers, Journal of Heat Transfer, 128(5) (2005) 427-433.
[39] H.W. Coleman, W.G. Steele, Experimentation, validation, and uncertainty analysis for engineers, John Wiley & Sons, 2018.
[40] Y. Chen, H. Yang, Y. Luo, Parameter sensitivity analysis and configuration optimization of indirect evaporative cooler (IEC) considering condensation, Applied Energy, 194 (2017) 440-453.